Simulation and Measurement of Narrowband Susceptibilities of Digital Automotive Sensors

Jan Benz, Jan Hansen
Robert Bosch GmbH
Reutlingen, Germany
jan.benz2@de.bosch.com

Stephan Frei
TU Dortmund University
Dortmund, Germany
stephan.frei@tu-dortmund.de

***Abstract*—Automotive sensors need to fulfill severe electromagnetic compatibility (EMC) requirements. To improve the robustness of a sensor in early product development stages, an accurate immunity simulation is essential. Furthermore, a fast and reliable broadband immunity measurement to cover all sensor susceptibilities is necessary.**

In this paper, a new approach to simulate the digital output values of a pressure sensor in a closed-loop Bulk Current Injection (BCI) procedure is introduced. In addition, a sensor specific measurement method of both high accuracy and short test time is presented. Finally, the simulations are validated with measurements using automotive pressure sensors.

***Index Terms*—Bulk Current Injection (BCI), Least Significant Bit (LSB), ADC Modeling, FM-measurement**

I. Introduction

Today's cars contain several dozens of sensors, controlling comfort functions (air conditioning etc.), drivetrain functions (exhaust after treatment, battery thermal management, etc.) as well as safety critical functions like the antilock braking system, the electronic stability control and the airbag system. In principle, many automotive sensors consist of two main components: A microelectromechanical system (MEMS) and an application-specific integrated circuit (ASIC). The MEMS converts a mechanical quantity (pressure, acceleration, yaw rate, etc.) into an electrical quantity. The ASIC processes and converts the often small MEMS currents and voltages by an analog-to-digital converter (ADC) and communicates with the electronic control unit (ECU). The connection between MEMS and ASIC, often called front-end, represents the most sensitive part of sensors [1], [2]. Fig. 1 illustrates the general setup of many automotive sensors. Many electromagnetic immunity

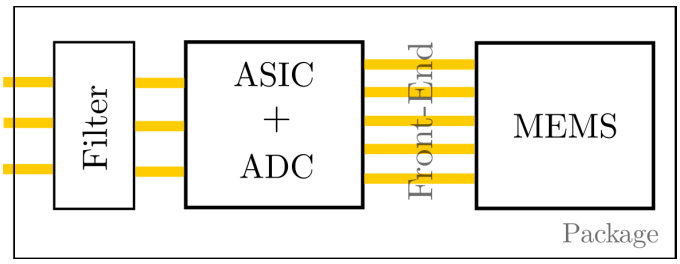

Fig. 1: Simplified schematic setup of many automotive sensors

tests have to be passed in the frequency range from some kHz up to several GHz. The closed-loop Bulk Current Injection (BCI) procedure is one of the harshest sensor tests applied mainly in the frequency range from 0.1 MHz - 400 MHz, due to the high power levels and the highly resonant setup (the mismatched wire harness causes sharp resonances). In this paper the closed-loop BCI procedure will be used as a test environment [3].

To cover the wide frequency range in an acceptable time, a continuous wave (CW) signal is used in general. Due to frequency steps larger than 1 MHz, which is a common step defined in many sensor test plans, many narrowband susceptibilities of the sensor cannot be measured reproducibly - which results in different test results. Solving this issue by reducing the frequency step width increases the test time dramatically from some minutes to several days, making measurements in a wide frequency range impossible.

Fast and accurate simulations can support the time consuming measurements. Furthermore, they enable a failure prediction, analysis and prevention in early development stages.

In this paper, two topics are addressed. First, a method to simulate the perturbation of the digital sensor signals during BCI is presented. Second, an improved sensor specific measurement method to speed up the measurement and support sensor immunity engineering is introduced.

II. System and Component Model

The simulated system consists of the BCI setup model, a passive sensor model and the analog-to-digital conversion model. BCI modeling has been investigated in many publications like [4], [5], [6], [7], [8]. The here used BCI modeling techniques are recapitulated shortly. In addition, a novel technique to accurately model the MEMS and ASIC within automotive sensors is presented. The investigation of an analog-to-digital converter (ADC) during EMC tests leads to a new way of directly simulating the sensors' digital signals.

A. BCI Test Setup

The BCI setup consists of injection and monitoring clamp, cable harness, ECU emulation (called loadbox), line impedance stabilization network (LISN) and the device under test (DUT) (here: digital automotive sensor) [3].

The models of the FCC F140 injection and the F65 monitoring clamp [9] are generated using the measurement and de-embedding based procedure shown in [4]. With the

978-1-7281-0594-9/19/$31.00 © 2019 IEEE

use of modal converters, presented in [5], universal, harness independent and measurement based clamp models can be derived without using 3D simulations. The harness is modeled using CST Cable Studio [10]. LISNs should show an input impedance of 50 Ω only up to 108 MHz. A complex resonant behavior, caused by the parasitic effects, appears for higher frequencies. The authors in [6] presented a method using S-parameter measurement and fixture de-embedding to generate LISN models up to 1 GHz.

The internal circuit of loadboxes changes with the different sensors. We therefore use hybrid models consisting of a 3D modeled housing and a circuit model of the internal components to guarantee high accuracy and flexibility for different sensors. In-depth information on sensor modeling is shown in the next section.

All components are finally assembled in CST Studio [10]. Additional variables (power calibration of the injection clamp, transfer impedance of the monitoring clamp, current limit (here: 300 mA)) are measured. A frequency domain simulation with a normalized 1 V excitation is performed. In a post-processing step, the closed-loop control is calculated. Fig. 2 shows the comparison between measurement and simulation of a 300 mA closed-loop BCI test up to 400 MHz using a floating pressure sensor. The simulation covers the measurements with a deviation smaller 10 mA up to 400 MHz. This validates the high quality of the proposed method.

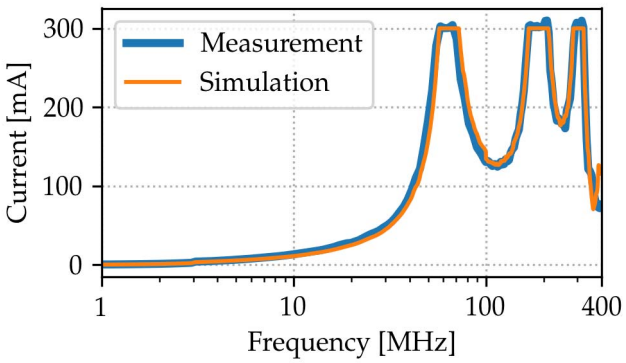

Fig. 2: Injected CM-current comparison between measurement and simulation during a 300 mA closed-loop BCI test

B. Sensor

This section introduces the modeling of major sensor components. Without loss of generality, all further steps will investigate automotive pressure sensors.

1) MEMS: The MEMS is the actual sensor element and consists, in case of a pressure sensor, of a resistive Wheatstone bridge as well as of a forward biased temperature diode. The piezo resistors and therefore the output voltage of the Wheatstone bridge change depending on the pressure. To include all parasitic field couplings, the functional, exterior layer of the MEMS and the bonds are modeled in 3D as shown in Fig. 3. Components and parasitics from internal, semiconducting layers are added using discrete elements.

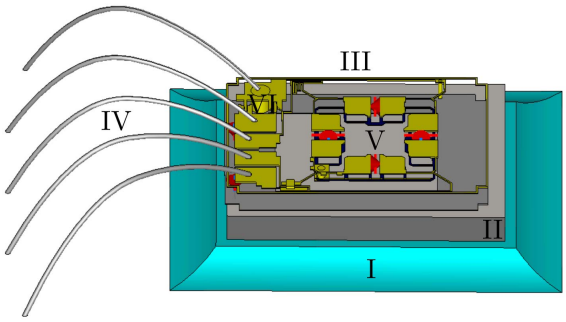

Fig. 3: 3D model of a pressure sensor MEMS (I) glue (II) substrate (III) functional layer (IV) bonds (V) Wheatstone bridge (VI) temperature diode

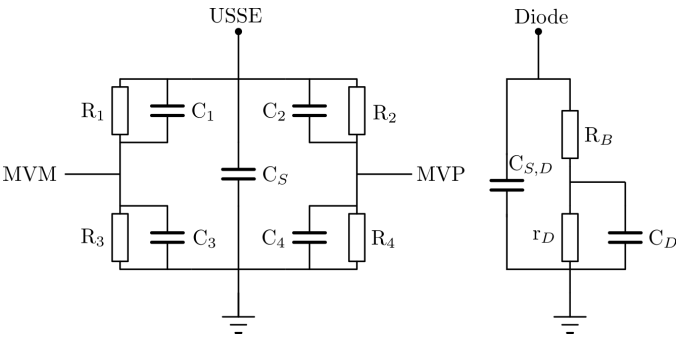

Fig. 4: Circuit model of the Wheatstone bridge (left) and the temperature diode (right) of the MEMS

Fig. 4 shows the circuit model of the MEMS element. Besides the piezo resistors $R_1 - R_4$, their associated parasitic capacitances $C_1 - C_4$ are included. The parasitic capacitance of the voltage supply (USSE) is represented by C_S. The center taps (MVM and MVP) of the Wheatstone bridge are connected to the ADC. To perform a simulation in the frequency domain, a small signal behavior of the temperature diode is assumed. Thus, the temperature diode can be described with the differential resistance [11]

$$r_D \approx \frac{n \cdot U_T}{I_D}, \tag{1}$$

the diffusion capacitance, which is dominant in the operation point [11]

$$C_D \approx \frac{\tau_T I_D}{U_T}, \tag{2}$$

the bulk resistance R_B of the doted layers, and the parasitic stray capacitance $C_{S,D}$. In Eq. (2) τ_T is the transit time, I_D is the forward drain current, U_T is the temperature voltage and n is the ideality factor of the diode.

2) ASIC with Analog-to-Digital Converter: Coupling relevant parts of the ASIC (bonds, pads, exposed pad, ground ring) are modeled in 3D as shown in Fig. 5. The capacitance between ground ring and the exposed pad is included with a discrete element.

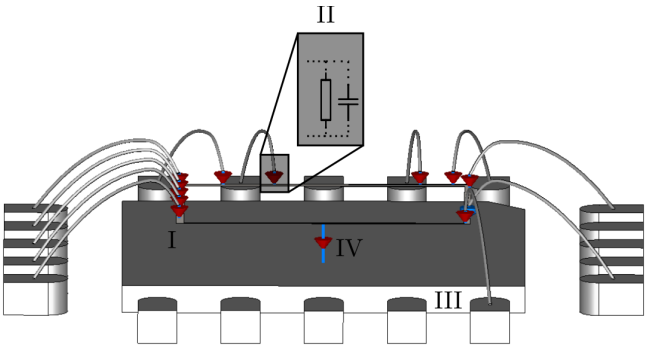

Fig. 5: Modeling structure of the ASIC (I) ground ring (II) RC termination (III) exposed pad (IV) internal ground capacitance

The internal impedances of the ASIC are described by the well-known method of Integrated Circuits Immunity Model-Conducted Immunity (ICIM-CI) [12] using a passive distributed network with an equivalent RC network to the internal ground ring. Internal voltage regulators are passively modeled at their operating point as shown in [13].

To digitalize the MEMS signals, many automotive sensors use switched-capacitor delta-sigma ($\Delta\Sigma$) analog-to-digital converters (ADCs) with a sampling frequency f_s between several hundred kilohertz and some megahertz. The principle behavior of a simplified switched-capacitor $\Delta\Sigma$-ADC is shown in Fig. 6. The functional behavior of such an ADC consists of two phases [14]:

- Phase 1: The switches S1 are closed (S2 opened) and the sampling capacity C_S is charged.
- Phase 2: The switches S1 are open and, after a small dead time, the switches S2 close. The charge stored in phase 1 is now transferred to the capacitor C_I.

Only during phase 1, an EMC noise can disturb the desired signal on the sampling capacitance. The active ADC characteristics are thus reduced to a passive RC network during phase 1. This is illustrated in Fig. 6. The resistance R_{on} of the complementary metal-oxide-semiconductor (CMOS) switches S1 can be derived as [11]

$$R_{on} = \frac{L}{\mu_n C_{ox} W (U_{GS} - U_{Th})} \tag{3}$$

with μ_n the electron channel mobility, U_{Th} the threshold voltage, L the channel length, W the channel width, C_{ox} the gate capacitance per unit area and U_{GS} the gate-source voltage.

In the investigated sensors, the resistance R_{on} reaches 5-10 kΩ and acts in combination with the sampling capacitance as a low pass for the injected EMC noise. The maximum deviation due to EMI appears when the switches S1 turn off

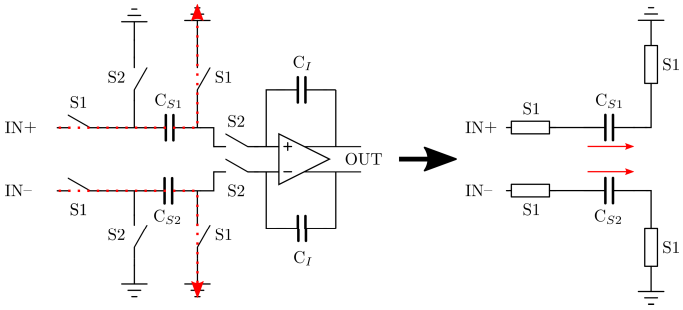

Fig. 6: Simplified functional model of the ADC (left) and the passive model during phase 1 (right).

TABLE I: Additional attenuation due to limited switching speed of a 5 ns fall-time CMOS

frequency	damping factor [%]	damping factor [dB]
1 MHz	99.3	0.06
10 MHz	85.6	1.35
100 MHz	37.0	8.64
400 MHz	7.9	22.05
1000 MHz	1.2	38.42

during the maximum or minimum of the harmonic noise on the sampling capacitor. The sensor output signal correlates with the differential voltages $U_{C_{S1}}$ and $U_{C_{S2}}$. Therefore, the voltage difference U_{ADC} of the noise amplitudes on the sampling capacitors C_{S1} and C_{S2} is observed.

C. LSB Calculation

The presented simplified model of the ADC is valid as long as

$$\frac{1}{T_{fall}} \gg f_{BCI}. \tag{4}$$

T_{fall} is the fall-time of the ADC switches and f_{BCI} is the oscillation time of the BCI clamp signal.

With a fall time of the investigated ADC switches between 1-10 ns, this assumption is valid up to several tens of MHz. In general, the fall time correlates with the sampling frequency of the ADC. For frequencies above this limit the BCI noise voltage cannot be seen as constant during the switching event anymore. In combination with the sampling capacitance, the turn off switching behaves as a time-variant low pass filter. The consequence is an additional attenuation.

To reproduce and to quantify this effect, the switching event is modeled in a simple time domain simulation of the ADC using a time-variant resistor as the switching CMOS. In addition, a phase sweep of the noise to extract the worst case of the turn off is performed. For infinitely fast switching this is obviously the maximum and minimum of the noise as mentioned above.

Table 1 shows the additional attenuation of a 5 ns fall-time CMOS compared to an infinitely fast CMOS switch. A non-linear curve (k_{att}) with respect to the frequency is fitted to

the extracted damping factor and is included as additional attenuation in a post-processing step. The differential voltage U_{ADC} (see Fig. 6) results as

$$U_{ADC} = (U_{CS1} - U_{CS2}) \cdot k_{att}. \tag{5}$$

To compare the simulated front-end voltages with measurements, a transformation into digital values, i.e. least significant bits (LSBs), is necessary. LSBs describe the smallest unit a sensor can measure. E.g. if the sensor can resolve 0.1 kPa and a deviation of 100 LSB is measured, the sensor measures an error due to EMI equivalent to 10 kPa. The same linear transformation applies to the temperature channel. All automotive sensors are specified to a maximum tolerable LSB deviation and are therefore evaluated with a kind of a digital peak detector.

To calculate the LSB, the following functional properties of MEMS and ASIC are needed:

- p_{sens}: The sensitivity p_{sens} of the MEMS describes the DC voltage change of the Wheatstone bridge in the presence of a pressure change. This property is given in mV/kPa.
- $\Delta p_{digital}(p)/\Delta p$: This fraction describes the change in LSB in the presence of a pressure change and is given in LSB/kPa.

In addition, for the temperature diode:

- T_{sens}: The sensitivity T_{sens} of the MEMS describes the DC voltage change of the temperature diode in the presence of a temperature change. This property is given in mV/K. For silicon diodes this property is -1,7 mV/K.
- $\Delta T_{digital}(T)/\Delta T$: This fraction describes the change in LSB in the presence of a temperature change and is given in LSB/K.

In a final step, all previous introduced steps are combined. Therefore, a complete closed-loop BCI simulation is performed. The voltage U_{ADC} in Eq. (5) is calculated in a post-processing step. Afterwards, the analog voltage U_{ADC} is combined with the above explained analog-to-digital transformation properties of the sensor.

Finally, the LSB deviation of the sensor can be calculated as

$$\Delta p[LSB] = \hat{U}_{ADC,p} \cdot \frac{\Delta p_{digital}(p)}{\Delta p} \cdot \frac{1}{p_{sens}} \tag{6}$$

for the pressure and

$$\Delta T[LSB] = \hat{U}_{ADC,T} \cdot \frac{\Delta T_{digital}(T)}{\Delta T} \cdot \frac{1}{1.7\,mV/K} \tag{7}$$

for the temperature. The presented procedure now enables the simulation of the digital signal deviation of automotive sensors. A direct comparison to results of BCI measurements can be seen at the end of the paper in Figs. 10 and 11.

III. Measurement

Due to the discrete sampling frequency f_s and the digital filters (FIR (finite impulse response) and IIR (infinite impulse response) in the digital signal processing (DSP) chain), only noise with the frequency

$$f = n \cdot f_s \pm \frac{f_{BW}}{2} \text{ for } n \in \mathbb{N}^* \tag{8}$$

can harm the sensor's output signals. Here, the bandwidth of the digital filters f_{BW} (IIR and FIR) is between several 100 Hz and some 1000 Hz.

The modulation specified in the standard is continuous wave (CW) with a logarithmic frequency step between 1 % and 10 % resulting in a frequency step width larger than 1 MHz. Due to the large steps, the narrowband susceptibilities cannot be found. Furthermore, depending on the step size and the sensor oscillator clock, the results can vary in each test.

If a narrowband susceptibility of the DUT is expected, the CW frequency step must be reduced, until the results are replicable und accurate. This causes the test time to increase from several minutes to days.

A. Frequency Modulation

To measure the narrowband susceptibilities with high reliability in the BCI range from 0.1-400 MHz and keep the test time low at the same time, a sensor specific frequency modulation (FM), based on [15], can be used. Instead of only testing specific frequencies with a CW signal, a slow FM is superimposed to cover the whole spectrum. Accordingly, the following parameters are considered:

- dwell time T_{dwell} per frequency step
- frequency step width f_{step}
- modulation frequency f_m
- deviation frequency f_Δ
- sensor data transfer rate f_{data}
- bandwidth of the susceptibility f_{BW}

To ensure a horizontal power spectrum of the frequency modulation and thus a constant frequency change, a triangular modulation is suitable. In order to cover the complete spectrum, while keeping redundancy at minimum, it follows that

$$f_{step} = 2 \cdot f_\Delta, \tag{9}$$

$$T_{dwell} = \frac{1}{f_m}. \tag{10}$$

The time domain modulation as well as the resulting spectrum can be seen in Fig. 7.

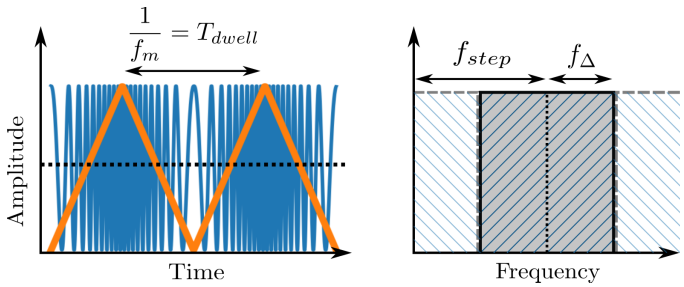

Fig. 7: Frequency modulation in time and frequency domain

Like in a peak detector, it is important to measure an adequate amount of samples within the narrowband susceptibility to detect the amplitude of the BCI noise. The measured quantity of samples n_s can be calculated as

$$n_s = \frac{f_{BW}}{f_{step} \cdot f_m} \cdot f_{data} \tag{11}$$

where the term $\frac{f_{BW}}{f_{step} \cdot f_m}$ describes the measured time within each narrowband susceptibility and f_{data} the amount of samples transferred per second.

Due to a random sampling of the BCI noise, a stochastic approach to calculate the minimum amount of samples n_s is needed. With the precondition to measure at least one value x greater 95 % of the sinusoidal BCI noise peak with a probability of 95 %, it follows that

$$P(x \geq 1) \geq 0.95 \mapsto P(x = 0) < 0.05. \tag{12}$$

With the probability mass function [16]

$$P(x = k) = \binom{n_s}{k} p^k (1-p)^{(n_s - k)}, \tag{13}$$

the probability p can be calculated as

$$p = 1 - \frac{sin^{-1}(0.95)}{\pi/2} = 20.2\%. \tag{14}$$

Finally, Eq. (12) is valid for $n_s > 14$. Therefore, at least 14 measured samples are mandatory in each narrowband susceptibility to cover 95 % of the sinusoidal BCI noise peak with a probability of 95 %. To fulfill that requirement with the help of Eq. (11), f_m and f_Δ must be determined appropriately.

B. Comparison

The new test procedure is tested on a pressure sensor with a sampling frequency f_s = 1.25 MHz and a bandwidth of the digital filters f_{BW} of around 3 kHz. The transfer protocol uses a transfer frequency f_{data} = 1.2 kHz. With the help of Eqs. (9) and (10), the frequency modulation is set to a modulation frequency of 1 Hz, a dwell time of 1 s, a deviation frequency of 100 kHz and a frequency step width of 200 kHz. Eq. (11) results in n_s = 18, which fulfills the requirement above.

Fig. 8 shows the comparison between the standard CW procedure (f_{step} = 200 kHz) and the enhanced frequency modulation. The CW procedure tests only some narrowband susceptibilities partly and randomly. Reliable testing of the narrowband susceptibilities can be seen when using the introduced FM. Each of the narrowband susceptibilities in Eq. (8) is tested and can be seen as a sharp LSB deviation peak.

Furthermore, Fig. 9 illustrates the accuracy of the frequency modulation compared to the standard CW method for a single narrowband susceptibility. In the CW procedure it is necessary to reduce the step to a width smaller 1 kHz to measure the maximum deviation accurately. It can be seen that frequency modulation reaches an accuracy close to the 1 kHz step CW test while having the test time reduced by a factor up to 200.

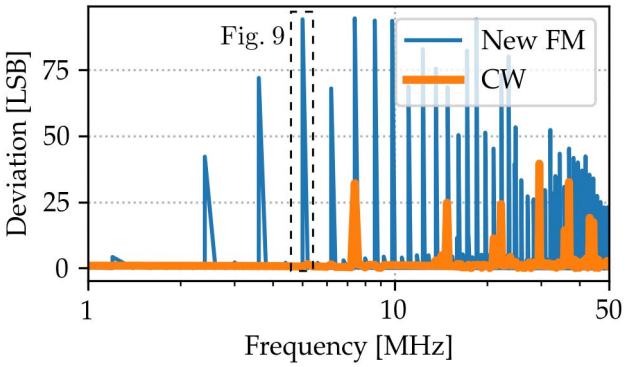

Fig. 8: Comparison between standard test procedure (f_{step} = 200 kHz) and the introduced FM (f_{step} = 200 kHz and f_m = 1 Hz) for sensor front-end coupling

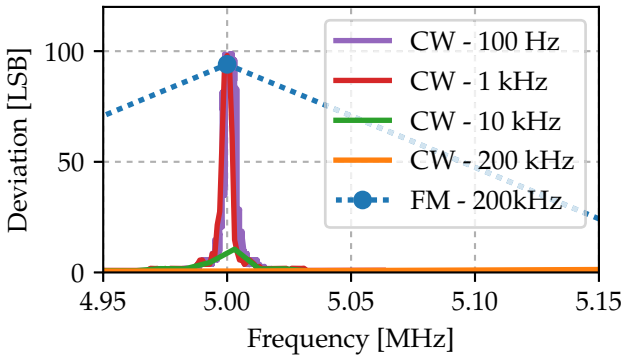

Fig. 9: Comparison between standard CW with varying f_{step} and frequency modulation (f_{step} = 200 kHz and f_m = 1 Hz) for a narrowband susceptibility with f_{BW} = 3 kHz

IV. System Model Validation

The previous sections presented a new method to directly simulate the deviation of the digital output values of automotive pressure sensors. Furthermore, a sensor specific test procedure for narrowband susceptibilities is shown. Finally, this section compares the previous steps. Therefore, the LSB of two different sensor setups (floating and locally grounded) are simulated and measured during a closed-loop BCI test. The LSB deviation for a pressure channel as well as a temperature channel is observed. Fig. 10 shows the maximum LSB deviation of the pressure signal up to 400 MHz. The deviation nearly disappears for frequencies above 50 MHz due to several stages of EMC filters. The simulated envelope of the digital error correlates well with the introduced FM measurement. A maximum discrepancy of only 20 LSB, which is equivalent to the very small voltage of $\Delta U_{LSB} = 300\,\mu V$, can be seen.

Fig. 11 shows the temperature channel LSB deviation of a locally grounded pressure sensor. Due to less filter stages

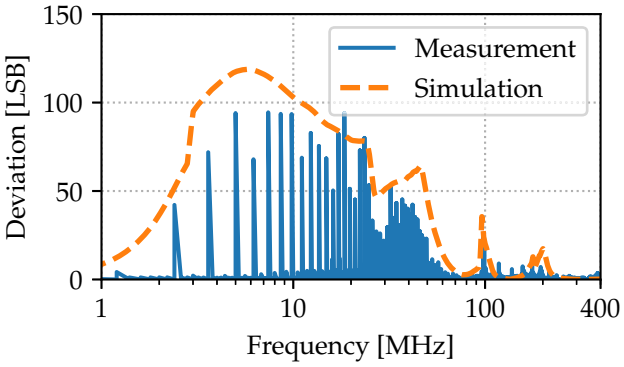

Fig. 10: Simulated and measured pressure channel LSB deviation during a 300 mA closed-loop BCI test

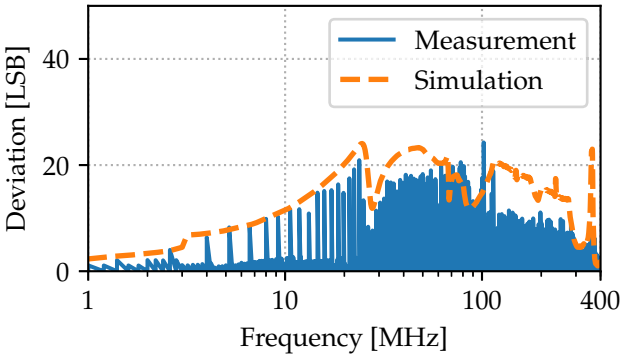

Fig. 11: Simulated and measured temperature channel LSB during a 300 mA closed-loop BCI test

in the temperature channel, the deviation is visible up to 400 MHz. A maximum deviation of only 10 LSB in the higher frequency range is visible, which can be improved by further investigating the active behavior of the switched-capacitor ADC.

The high accuracy of the proposed model enables simulation based assessment and improvement of narrowband sensor susceptibilities in early development stages.

V. Conclusion

This contribution presents the modeling and simulation of digital sensor signal deviations due to electromagnetic coupling in the sensor front-end in BCI testing. Accurate immunity simulations enable an evaluation of different sensor concepts in early product development stages. The reduction of complex active sensor components (MEMS, ASIC and ADC) to passive, for the EMC simulation relevant parts is validated.

In addition, the paper presents a sensor specific measurement procedure to ensure reliable broadband immunity measurements on sensors with narrowband susceptibilities. An optimized frequency modulation reaches high accuracy compared to the common CW procedure while having a reasonable test time.

Simulations of a pressure and a temperature channel of different terminated sensors show high correlation to FM measurements and validate the presented simulation methods.

References

[1] V. Petkov, G. Balachandran, and J. Beintner, "A fully differential charge-balanced accelerometer for electronic stability control," in *IEEE Journal of Solid-State Circuits*, vol. 49, pp. 380–381, 2014.

[2] F. Fiori, "EMI-induced distortion of baseband signals in current feedback instrumentation amplifiers," *in IEEE Transactions on Electromagnetic Compatibility*, vol. 60, pp. 605–612, 2018.

[3] ISO 11452-4: *Road vehicles – Component test methods for electrical disturbances from narrowband radiated electromagnetic energy, part 4: Harness excitation methods*, 2011.

[4] S. Miropolsky, A. Sapadinsky, and S. Frei, "A generalized accurate modelling method for automotive Bulk Current Injection (BCI) test setups up to 1 GHz," on 9th International Workshop on Electromagnetic Compatibility of Integrated Circuits – EMC Compo, pp. 63–68, 2013.

[5] M. Gonser, "EMV-Systemsimulation mit realen Kabelbäumen von Mess- und Prüfverfahren für Kfz-Komponenten," doctoral dissertation, Universität Erlangen-Nürnberg 2011.

[6] Y. Kondo, M. Izumichi, and O. Wada, "Simulation of Bulk Current Injection test using integrated circuit immunity macro model and electromagnetic analysis," on International Symposium on Electromagnetic Compatibility – EMC Europe, pp. 118–122, 2016.

[7] S. Miropolsky, A. Sapadinsky, and S. Frei, "Measurement-based circuit modeling of conducted and radiated automotive immunity test setups," on International Symposium on Electromagnetic Compatibility – EMC Europe, pp. 1305–1310, 2014.

[8] Y. Kondo, M. Izumichi, and O. Wada, "Simulation of Bulk Current Injection test for automotive components using electromagnetic analysis," *in IEEE Transactions on Electromagnetic Compatibility*, vol. 60 , pp. 866–874, 2018.

[9] Fischer Custom Communication, Inc., www.fischercc.com.

[10] CST Studio Suite 2018, www.cst.com.

[11] U. Tietze, C. Schenk, and E. Gamm, *Electronic Circuits: Handbook for Design and Application*, Springer-Verlag Berlin Heidelberg, 2008.

[12] IEC 62433-4:2016: *EMC IC modelling–Part 4: Models of integrated circuits for EMI behavioural simulation conducted immunity modeling (ICIM-CI)*, 2015.

[13] B. Crovetti and F. Fiori, "A linear voltage regulator model for EMC analysis," *in IEEE Transactions on Power Electronics*, vol.22, pp. 2282–2292, 2007.

[14] M. Huang and S. Liu, "A fully differential comparator-based switched-capacitor $\Delta\Sigma$ modulator," *in IEEE Transactions on Circuits and Systems II: Express Briefs*, vol. 56, pp. 369–373, 2009.

[15] C. Spindler, "New EMC-testing-method for smart sensors during for IC-design-process," on International Symposium on Electromagnetic Compatibility – EMC Europe, pp. 1186–1189, 2014.

[16] "Binomial distribution", Retrieved January 15, 2019, from https://en.wikipedia.org/wiki/Binomial_distribution.